IJE TRANSACTIONS B: Applications Vol. 35, No. 05, (May 2022) 943-953

International Journal of Engineering

Journal Homepage: www.ije.ir

Numerical Investigation of Geometric Parameters Effects on Heat Transfer Enhancement in a Manifold Microchannel Heat Sink

M. R. Babaei, G. A. Sheikhzadeh*, A. A. Abbasian Arani

Department of Mechanical Engineering, University of Kashan, Kashan, Iran

P A P E R I N F O

Paper history:
Received 15 January 2022
Received in revised form 05 February 2022
Accepted 10 February 2022

Keywords:
Manifold Microchannel Heat Sink
Thermophysical Properties
Heat Transfer Enhancement
Performance Evaluation Criterion

A B S T R A C T

Microchannel heat sink has been employed and as a part of electronic equipment extensively investigated. In this investigation, heat transfer and fluid flow features of laminar flow of water in a manifold microchannel heat sink (MMHS) was numerically simulated. Selected heat flux was 100 W/m^2 and water was as working fluid. The effect of length of inlet/outlet ratio ($\lambda=L_{inlet}/L_{outlet}$), the height of microchannel (H_{ch}), and width of the microchannel (W_{ch}) at Reynolds number (Re) range from 20 to 100 as independent parameters on the fluid flow and heat transfer features were examined. Obtained results demonstrate that in MMHS, the impinging jet on the bottom channel surface, inhibits the growth of hydrodynamic and thermal boundary layers, resulting in an enhanced heat transfer rate. Also, by increasing Re and keeping the geometric parameters constant, the heat transfer rate increases. Based on the present investigation, for low Re, it is better to choose a $\lambda=L_{inlet}/L_{outlet}>1$ and for high Re, choose a $\lambda<1$. For low Re, maximum of performance evaluation criterion (PEC_{max}) is obtained at H_{ch}=300μm, and for high Re, PEC_{max} is obtained at H_{ch}=240μm. for Re=20 to 100, the maximum of PEC_{max} is 1.765 and obtained at Re=100 and H_{ch}=240μm.

***doi**: 10.5829/ije.2022.35.05b.10*

NOMENCLATURE

W_{ch}	width of the microchannel (μm)	q''	heat flux (W/m^2)
W_f	width of the fin (μm)	Re	Reynolds number
H_{ch}	height of microchannel (μm)	T	temperature (K)
H_m	height of manifold (μm)	T_{in}	Inlet temperature (K)
H_s	height of substrate (μm)	T_{out}	Outlet temperature (K)
L_{in}	length of inlet path (μm)	T_m	mean Bulk temperature (K)
L_m	length of manifold (μm)	$\overline{T}_s$	average temperature of microchannel wall (K)
L_{out}	length of outlet path (μm)	u	velocity (m/s)
λ	length of inlet/outlet ratio (L_{inlet}/L_{outlet})	u_{in}	Inlet velocity (m/s)
MMHS	manifold microchannel heat sink	L	Length of microchannel (μm)
MMHE	manifold microchannel heat exchanger	Nu_{ave}	average Nusselt number
TMHS	Traditional microchannel heat sink	$Nu_{ave.r}$	reference average Nusselt number
PEC	performance evaluation criterion	f	friction coefficient
FFMHS	Force-fed microchannel heat sink	f_r	reference friction coefficient
JIHS	Jet impingement heat	k_f	thermal conductivity of fluid (W/mK)
p	Pressure (Pa)	μ_f	dynamic viscosity (Ns/m^2)
Δp	pressure drop (Pa)	c_p	specific heat capacity (J/kg K)
ṁ	mass flow rate (kg/s)	A_{ch}	Microchannel cross section (m^2)

*Corresponding Author Institutional Email: sheikhz@kashanu.ac.ir (G. A. Sheikhzadeh)

Please cite this article as: M. R. Babaei, G. A. Sheikhzadeh, A. A. Abbasian Arani, Numerical Investigation of Geometric Parameters Effects on Heat Transfer Enhancement in a Manifold Microchannel Heat Sink, ***International Journal of Engineering, Transactions B: Applications***, Vol. 35, No. 05, (2022) 943-953

1. INTRODUCTION

In the electronic equipment industry, using microchannel heat sink as one of the effective methods for achieving high electronic components thermal performance. Therefore, modeling different types of microchannel heat sink is one of the important topics of interest of researchers [1-3]. Also, Attempts had been made by many authors to develop improved models suitable for various proceses [4-6].

Traditional microchannel heat sink (TMHS) and manifold microchannel heat sink (MMHS) are two categories of the microchannel heat sink. TMHS has two fundamental problems: major variation of temperature within the heat source and high-pressure drop. In the MMHS, compared with TMHS, as shown in Figure 1, the coolant flow path to a small part is reduced, and also cold fluid impinges on the microchannel bottom surface. Therefore, the pressure drop is reduced, and the growth of thermal and hydrodynamic boundary layers is limited and leads to better heat transfer. Many researches have been done on the application of MMHS in the electronics industry and for the purpose to cool the electronic chips. At present, researchers are now trying to find MMHS that can not only improve heat transfer but also be economically viable and have a low pressure drop. Therefore, they are studying on MMHS geometry and etc. Some of these studies are discussed as follows:

Kermani [7] by experimental method, showed major enhancement in heat transfer coefficient in the MMHS for cooling the solar cells than TMHS. His result showed that for MMHS, 37% of total pressure drop were obtained in the microchannel with a hydraulic diameter of 36 µm and 13% of total pressure drop were obtained in the microchannel with a hydraulic diameter of 67 µm. The remaining total pressure drop occurs in the manifold. Escher et al. [8] introduced a 3D flow modeling of MMHS. They studied the hydrodynamics performance and thermal performance for one-unit cell of MMHS. Also, they determined thermal performance and total hydrodynamical structure of the system. Their observations showed that the width of the channel and L_{inlet}/L_{outlet}, change the thermal performance. Cetegen [9] for achieving the minimum pumping power and maximum heat transfer coefficients, by numerical simulation studied tree type of microchannel heat sink: Force-fed microchannel heat sink (FFMHS), TMHS, and Jet impingement heat sink (JIHS). Her results showed that at the same pumping power, for FFMHS, heat transfer coefficients are 306% higher than JIHS and are 72% higher than TMHS. Kasten et al. [10] for microchannel unit cell, numerically modeled a 3D conjugate heat transfer. In the next step, they simulated a 3D complete heat sink model. They concluded that if the flow rate increases, the thermal resistance of MMHS decreases and, pressure drop increases. Boteler et al. [11] by a numerical analysis and one phase mode, studied flow field and heat transfer for a manifold microchannel heat exchanger. They concluded that two parameters, such as a microchannel fin and width of microchannel, have a significant effect on thermal performance. Husain and Kim [12] numerically modeled a 3D model of MMHS. The key parameters of their research were thermal resistance and water pumping power. Their results showed that the nozzle height to the microchannel height (H_{nz}/H_{ch}) and the ratio of the microchannel width to the microchannel height (W_{ch}/ H_{ch}) are more effective parameters on pumping power of water and thermal resistance. Sarangi et al. [13], by 3D numerical simulation, studied the influence of geometrical variables such as manifold height, manifold inlet/outlet ratio, microchannel width, and microchannel depth on the performance of MMHS. Their study consisted of two sections: porous-medium pattern and unit-cell pattern. Their observations showed that the optimum value of the manifold inlet/outlet ratio is equal to 3. In the study of Arie et al. [14] the air was used as a cooling fluid in MMHS. To obtain the best design variables, they used an optimization function. Their investigation showed that, by using MMHS, improvement in heat sink thermal performance is observed. Arie et al. [15] for achieving

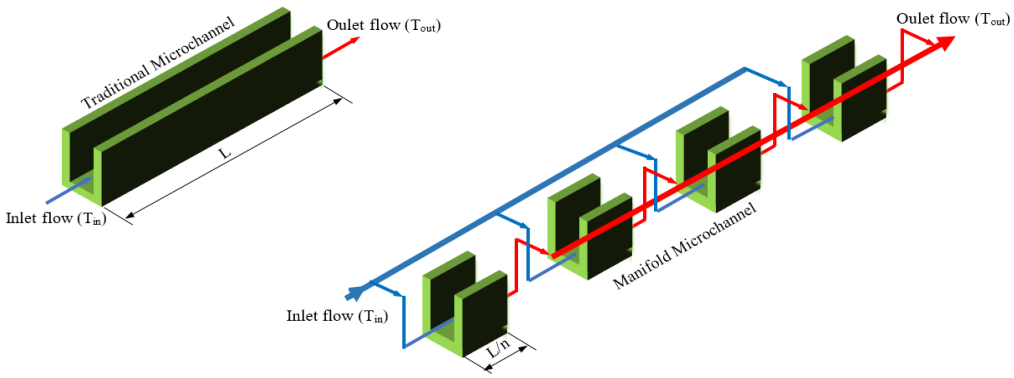

Figure 1. Comparison of Traditional microchannel with Manifold microchannel

the optimal thermal performance of manifold microchannel heat exchanger (MMHE) and for determining the best design parameters, used a numerical method. Their observations showed that friction coefficient and Nusselt number compared to chevron categories of the plate heat exchanger are effective parameters in optimizing the manifold microchannel. Yue et al. [16] studied thermal performances of a MMHS in the presence of nanofluids as working fluids. Their observations showed that Nusselt number and water pumping power increases by increasing the volume fraction of nanoparticles and Re and decreases by increasing the diameter of the particles. Andhare et al. [17] designed a particular type of MMHE to study numerically and experimentally the impact of this type of microchannel heat sink on thermal performance. Their observations showed that for $\dot{m}$<20g/s, the total heat transfer coefficient h_{total}=20000. W/m^{2}K was obtained. Li et al. [18] numerically studied flow field and heat transfer for both MMHS and TMHC for non-Newtonian fluid such as dilatant fluid and pseudo-plastic fluid. Their result showed that drag resistance decreased for pseudo-plastic fluid flow up to 2 orders and increased for dilatant fluid flow up to 3 orders. Arie et al. [19] enhanced the performance of an air-water MMHE, used multi-objective optimization and compared the results with optimized conventional heat exchangers, such as louvered fin, plain plate-fin, pin fin, wavy fin and, wavy fin surfaces. Their results showed that the sophisticated design of the manifolds and fins could significantly improve the performance of MMHE. Compared to a wavy-fin heat exchanger, MMHE can up to 60% increase heat transfer density.

Drummond et al. [20] experimentally studied a hierarchical MMHC. They studied the effect aspect ratio and channel width on the thermal and hydraulic performance. They showed that the case with a larger hydraulic diameter compared to the case with a smaller hydraulic diameter lead to lower thermal resistance and higher heat transfer coefficient. Ju et al. [21] presented numerical modeling to analyze thermal and hydrodynamic performances of the micro-pin-fin heat sink. Their result showed that heat sinks with square and circular micro-pin-fins with the same cross-sectional area have the same thermal performance. Zhang et al. [22] by numerical simulation, studied both steady and pulsating flow in MMHS. Their result showed that pulsating flow inlet, in comparison to the steady flow, improves thermal performance. Also, in comparison to other pulsating types, sinusoidal-wave pulsating flow plays a more effective role in enhancing heat transfer. Jung et al. [23] studied experimentally and numerically a 3D MMHS was made of silicon. Their experimental result showed that at a flow rate of 0.1 l/min and a maximum temperature of 90 C$^\circ$, 250 W/cm^2 is removed by the MMHS with a pressure drop of less than 3 kPa. Tiwari et al. [24] designed and studied experimentally single-phase flow in a MMHE. Their result showed that for the tube-side with $\dot{m}$=806 g/s and for the shell-side with $\dot{m}$=82 g/s, shell-side heat transfer coefficient of 45,000 W/m^2K and overall heat transfer coefficient of 22,000 W/m^2K can be obtained. Luo et al. [25], studied heat transfer in a MMHS for two-phase flow boiling process. Their observations showed that for the manifold divider, the manifold ratio ranges from 1 to 2 is suitable to reduce the pressure drop of the MMHS. Yang et al. [26] numerically studied performance enhancement of hybrid microchannel heat sink. Their result showed that compared to the usual MMHS, the best heat sink could decrease thermal resistance by 19.15% and reduce pressure drop by 1.91% at Re = 295. Drummond et al. [27] experimentally studied two-phase flow morphology in high aspect ratio manifold microchannels. Their results showed that for manifold microchannels, the two-phase flow regime plays an important role in heat transfer improvement and must be with accuracy considered in heat sink design. Luo et al. [28] by 3D numerical methods, studied two-phase flow boiling in MMHS for different manifolds configurations (C-type, H-type, Z-and, U-type). Their results showed that compared with C-type and Z-type, H-type and the U-type manifolds due to their lower pressure drop and better heat transfer performance are recommended. Yang et al. [29] performed an experimental comparison between a hybrid microchannel heat sink (HMHS) and a typical manifold microchannel heat sink (CMMHS. Their results showed that the HMHS reduce thermal resistance and pressure drop. Luo et al. [30] studied numerically pressure loss and thermal performance of subcooled flow boiling in an MMC with various sizes of fin widths and channel widths and various inlet volume flow rates. Their observations showed that the thermal resistance of heat sink reduced when the volume flow rate increases, but pressure drop increased.

In the current study, the effects of variation of geometric dimension of MMHS such as length of inlet/outlet ratio, the height of microchannel and, width of microchannel at Re=20 to 100 on the flow field and heat transfer to find the optimal geometric dimension are numerically investigated. According to the obtained results, the best geometry is selected in terms of thermal improvement. In addition, for more precise results, the water thermophysical properties of the working fluid and silicon as a solid part (manifold and microchannels) are considered temperature-dependent, which had not been considered in previous similar articles. The PEC is also considered as a criterion for selecting the optimal microchannel rather than Nusselt number, and pressure drop.

At first of the current investigation, the model under consideration and boundary condition are presented. Then, system of governing equations and boundary conditions, numerical procesure, gind independency study and validation are done. Finally results and disscussion are presented for investiagatoin of heat transfer and fluid flow features of laminar flow of water in a manifold microchannel heat sink. Figure 2 shows the research methodology.

2. MODEL DESCRIPTION

2. 1. Geometrical Model and Boundary Conditions

The effect of variable geometric parameters such as λ, H_{ch} and W_{ch} for Re=20 to 100 on the flow field and heat transfer was investigated. Manifolds, microchannels and substrate are made of silicon. MMHS schematic in the current study is shown in Figure 3. The manifolds are distributed above the microchannels. The coolant fluid, after passing through the inlet channels of the manifolds, rotates 90° and enters the microchannels, removes the heat from the substrate along the microchannel length and, finally 90° turn and exits upward and enters the output channels in the manifold. Figure 4 shows the computational domain and geometric dimension for a unit cell of MMHS. Due to symmetry boundary conditions and to reduce the computational cost, a unit cell of MMHS is chosen. At the inlet of manifold, mass flow inlet and, at the outlet of manifold, pressure outlet have been selected as boundary conditions. Also, constant heat flux of 100 W/cm^2 on the bottom wall and no-slip velocity boundary condition on the walls of the microchannel has been considered. Figure 5 indicates the boundary conditions for the unit cell of MMHS.

3. THERMOPHYSICAL PROPERTIES

In the present simulation, silicon has been used as a solid part (manifold and microchannels) and, water is used as a working fluid. Temperature-dependent thermophysical properties between 300K to 400K, including thermal conductivity and dynamic viscosity of water and thermal conductivity of silicon were considered as the function of temperature [31-32]. Variations of the other

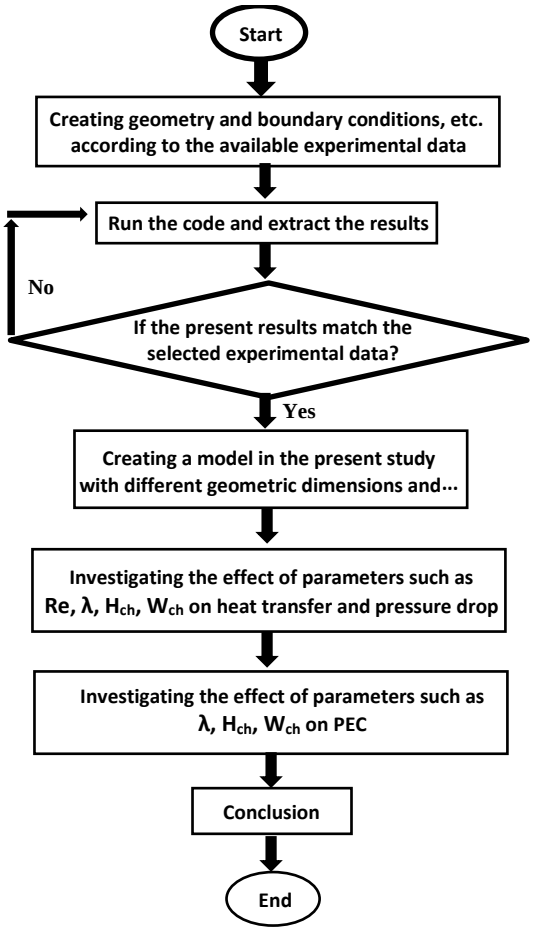

Figure 2. Research methodology

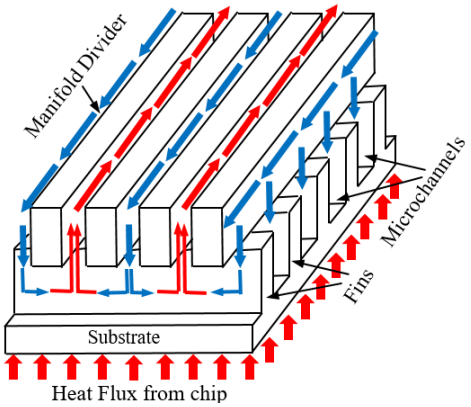

Figure 3. Schematic of MMHS

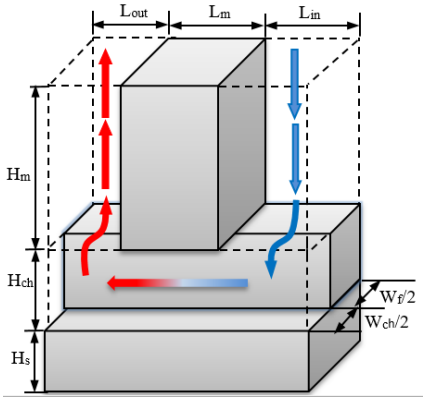

Figure 4. Computational domain and geometric dimension for the unit cell of MMHS

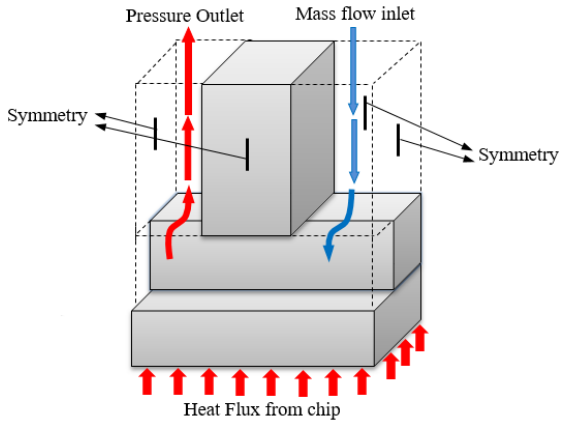

Figure 5. Applied boundary conditions for the unit cell of MMHS

thermophysical properties of water and silicon between the temperature ranges of 300K to 400K have no significant effect on the results.

4. GOVERNING EQUATIONS

Single-phase fluid flow and laminar flow governing equations at steady states condition in Cartesian coordinate is:
Continuity equation:

$$\frac{\partial}{\partial x_j}(u_j) = 0 \tag{1}$$

Momentum equation:

$$\frac{\partial}{\partial x_j}(\rho u_j u_i) = -\frac{\partial p}{\partial x_i} + \frac{\partial}{\partial x_j}(\mu_f \frac{\partial u_i}{\partial x_j}) \text{ (fluid)} \tag{2}$$

Energy equation:

$$\frac{\partial}{\partial x_j}(\rho u_j c_p T_f) = \frac{\partial}{\partial x_j}(k_f \frac{\partial T_f}{\partial x_j}) \text{ (solid)} \tag{3}$$

T , p ,and u_j represent the temperature, pressure, and velocity, while the subscripts f and s refer to the fluid and solid, respectively. For the flow to justify the assumption of laminar flow, the low Re (Re=20 to 100) is considered. The liquid to the solid interface was coupled by continuity of both heat flux and temperature:

$$T_{s_{interface}} = T_{f_{interface}} \tag{4}$$

$$-k_s \left(\frac{\partial T_s}{\partial n}\right)_{interface} = -k_f \left(\frac{\partial T_f}{\partial n}\right)_{interface} \tag{5}$$

4. 1. Important Parameters in the Three-dimensional Flow The friction coefficient, which is one of the parameters for evaluation of the microchannel operation, is defined as follows:

$$f = 2\Delta p \frac{D_h}{L} \frac{1}{\rho u_{in}^2} \tag{6}$$

where, L, D_h, u_{in}, and ρ are the length, hydraulic diameter, inlet velocity, and density, respectively.
The average Nusselt number defined as follows:

$$Nu_{ave} = \frac{q'' D_h}{k_f(\overline{T}_s - T_m)} \tag{7}$$

where, T_m and $\overline{T}_s$ are the mean Bulk temperature and microchannel wall temperature, respectively.
Performance Evaluation Criterion parameter (PEC), is defined as follows [33]:

$$PEC = (Nu_{ave}/Nu_{ave.r})/(f/f_r)^{1/3} \tag{8}$$

Re based on flow in the straight part of the microchannel according of Figure 6 defined as follows:

$$Re = \frac{\dot{m}_{ch} D_h}{\mu A_{ch}} \tag{9}$$

where

$$A_{ch} = w_{ch}/2 \times H_{ch} \tag{10}$$

$$D_h = \frac{2H_{ch}w_{ch}}{H_{ch}+w_{ch}} \tag{11}$$

5. GRID INDEPENDENCY

Several meshes with different cell numbers have been used to ensure that the results are independent of the grid. The mesh and results are plotted for the microchannel middle plate. According to Figure 7, for one case, a mesh with the 1420800 cells is sufficient for conducting simulation. By increasing the cell numbers more than 1420800, the obtained results do not have significant variations (heat transfer coefficient difference between 1420800 and 1965600 cells is 0.50%).

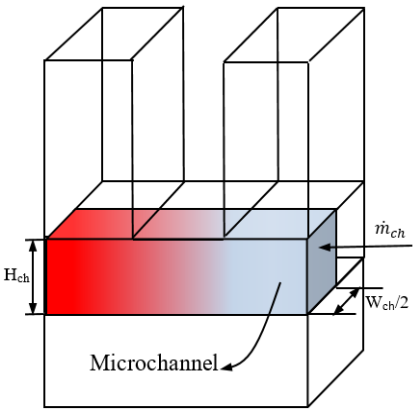

Figure 6. Microchannel section and microchannel geometrical characteristics

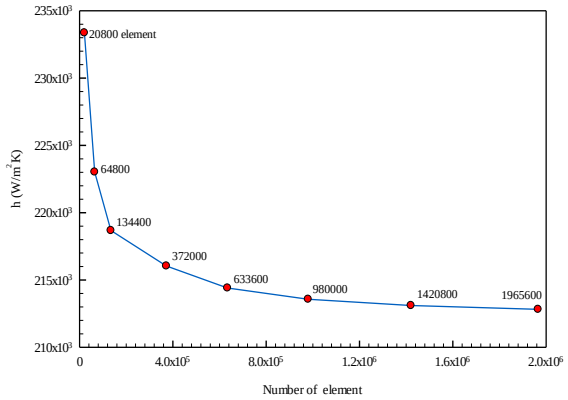

Figure 7. Mesh independence study. Hch = 360µm, Wch=60µm

6. MODEL VALIDATION

For assurance of the accuracy of numerical simulations, the numerical results are compared with available experimental data. In Kermani's study, heat transfer enhancement of MMHS with hydraulic diameter D_h=36µm examined. Figure 8 show validation with kermani result for D_h=36µm. according to Figure 7, it can be seen that the current results have good match with Kermani's experimental data [7].

7. RESULTS AND DISCUSSIONS

In this section, the results of the numerical simulation of fluid flow and heat transfer inside the MMHS are presented. Nu and Δp are two important parameters that are presented. Also, to study from an engineering and economic viewpoint, the PEC has been presented for different cases. Also, the results are presented as temperature contours and velocity contours.

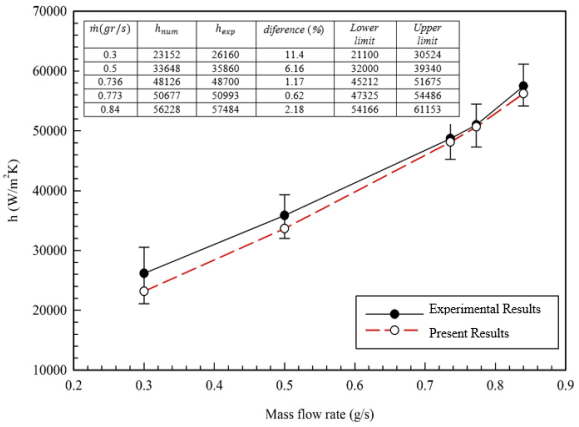

Figure 8. Heat transfer coefficient variations versus mass flow rate: comparison of present numerical results with experimental result [7] for D_h=36µm

7. 1. Effect of Re on Heat Transfer and Pressure Drop

The cooling fluid, after passing through the inlet nozzle, impacts the microchannel floor. In the MMHC flow, due to the direct impact of the flow perpendicular to the microchannel floor and the short flow path length, most of the flow is developing along the microchannel, thus limiting the growth of the hydrodynamic and thermal boundary layer. Therefore, a small diffusion length from the solid wall to the convective flow and better heat transfer rate is achieved. At the subsequent region, the rate of heat transfer decreases due to the growth of the hydrodynamic and thermal boundary layer. The results are plotted for the microchannel middle plate. Figure 9 shows temperature contours and velocity contours at various Re for H_{ch}=600µm, W_{ch}=60µm, W_f=60µm, L_{in}=120µm, and L_{out}=200µm. According to Figure 9(a), as the Re increases, the temperature of the microchannel floor and, consequently, the surface temperature in contact with the heat source decreases; this is due to the increase in flow rate and fluid velocity on the microchannel floor. The maximum temperature of the microchannel floor is 311.3K at Re=20 and is 306.3K at Re=100. Also, the thermal and hydrodynamic boundary layer thickness is reduced, and therefore, the heat transfer rate is increased. At the inlet zone of the flow from the nozzle to the microchannel, due to the reduction of cross-section, the velocity in this zone increases (according to Figure 9(b)) and formed a rotational zone near this zone. The Muximum velocity is related to the microchannel input at Re=20 is 1.07m/s and at Re=100 is 5.27m/s. Also, by increasing the Re, the flow injection velocity on the microchannel floor increases, and the formed rotational zone becomes larger.

7. 2. Effect of λ =L_{inlet}/L_{outlet} on Heat Transfer and Pressure Drop

Figure 10 shows temperature contours and velocity contours at various λ for H_{ch}=600µm, W_{ch}=60µm, W_f=60µm and L_{out}=200µm at Re=100. Studies were performed for λ =0.6 to 1.3, but contours from λ=1 to λ=1.3 are similar, and their changes are not significant and not shown. Figure 10(a) shows that by increasing in λ, the temperature of the microchannel floor increases. Due to the increase in cross-sectional area and decrease in inlet velocity from the nozzle to the microchannel, the flow injection velocity on the microchannel floor decreases. The maximum temperature of the microchannel floor is 306.3K at λ=0.6 and is 307.8K at λ=1. Figure 10(b) show with an increase in λ, inlet velocity from the nozzle to the microchannel decreases, and as a result, flow injection velocity on the microchannel floor decreases. The input velocity at λ=0.6 is 5.27m/s and at λ=1 is 3.45m/s. Also as λ increases, the maximum velocity zone is also seen in the output manifold, and in λ=1, the maximum velocity is seen in the output manifold zone.

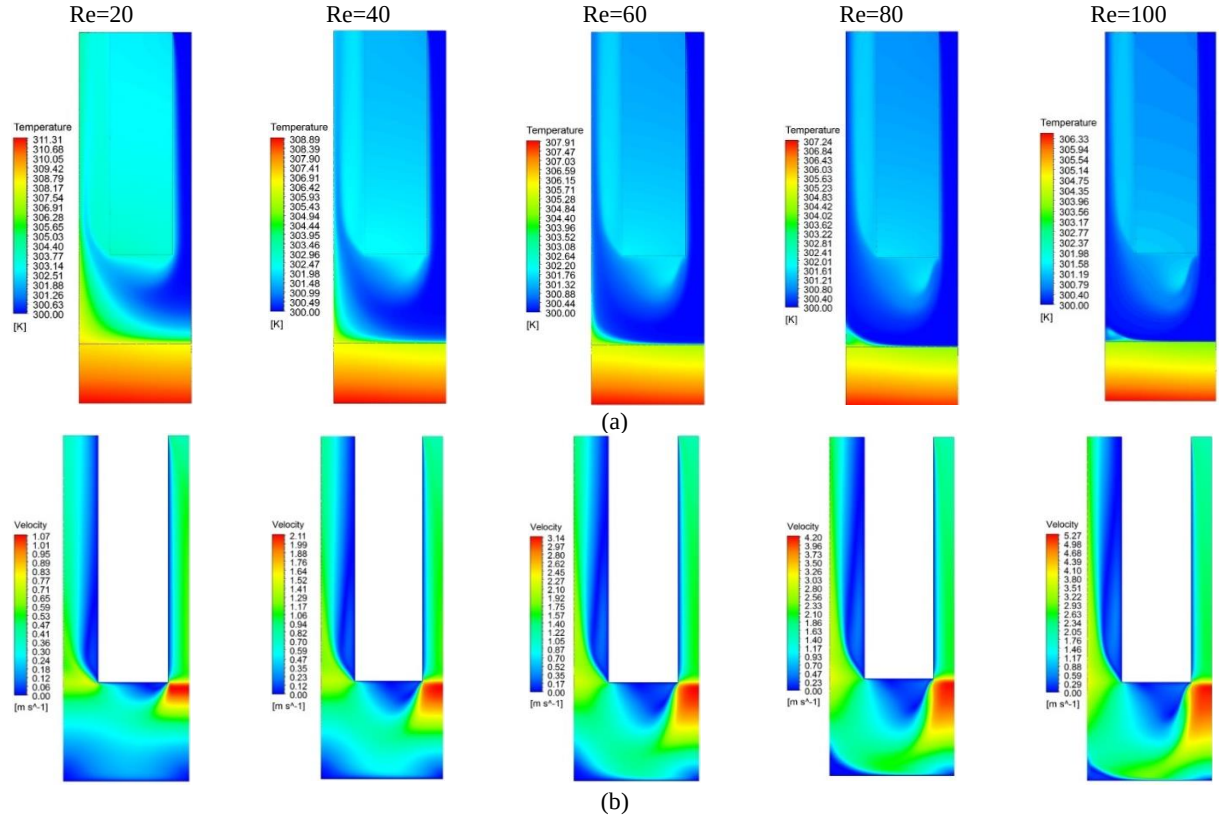

Figure 9. (a)Temperature contours (b) Velocity contours at various Re

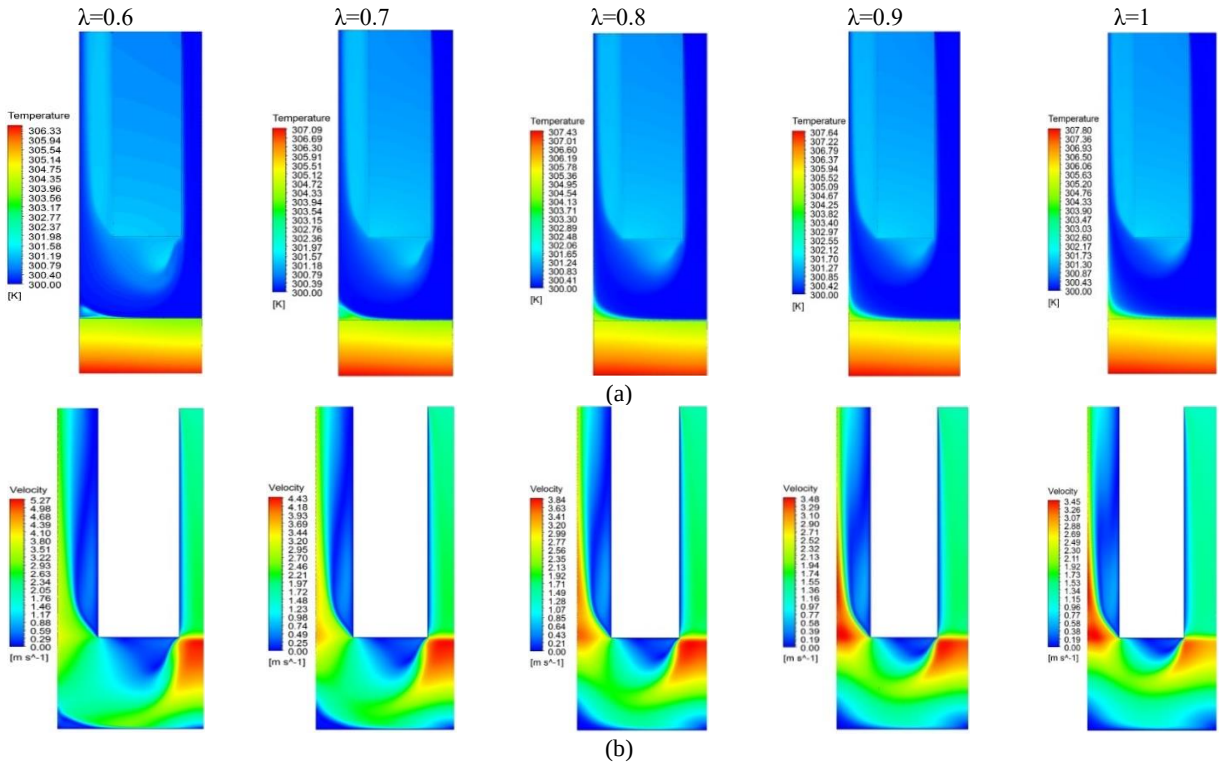

Figure 10. (a)Temperature contours (b) Velocity contours at various **λ**

Figures 11(a) and 11(b) respectively show variations of the Nu and Δp versus λ for different Re on the microchannel floor. By increasing Re, Nu and Δp are increased. At higher Re and smaller λ, the slope of variations of Nu and Δp is greater and for lower Re the slope of the changes is imperceptible. By increasing in λ, the amount of Nu and Δp, as well as their variations are reduced.

7. 3. Effect of λ on PEC Figure 12 shows PEC for various λ and Re. by increasing λ, PEC is increased for Re=20, 40 and 60 and for λ>1, PEC variations are insignificant. For Re=80, the PEC values are close to 1. For Re=100, by increasing in λ, PEC is decreased. The highest PEC is occurred at Re=100 and λ=0.6. It seems that due to the smaller inlet section of the microchannel at λ=0.6 than other λ values, with increasing Reynolds number, the increase in heat transfer is greater than the pressure drop increase. For lower Re, it is better to choose a λ>1 and for higher Re, choose a λ<1.

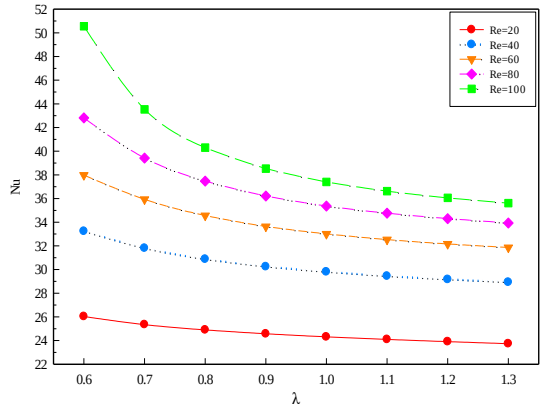

(a)

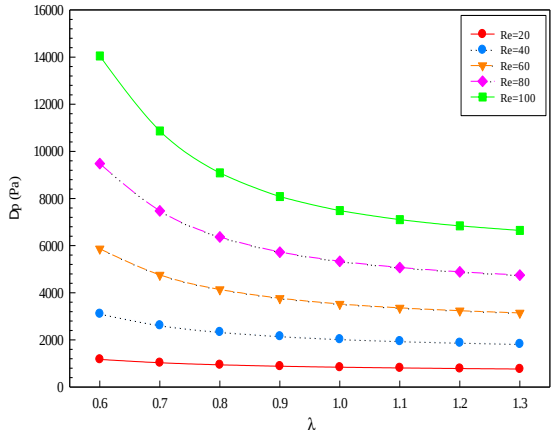

(b)

Figure 11. Variations of the (a) Nu (b) Δp versus λ for various Re

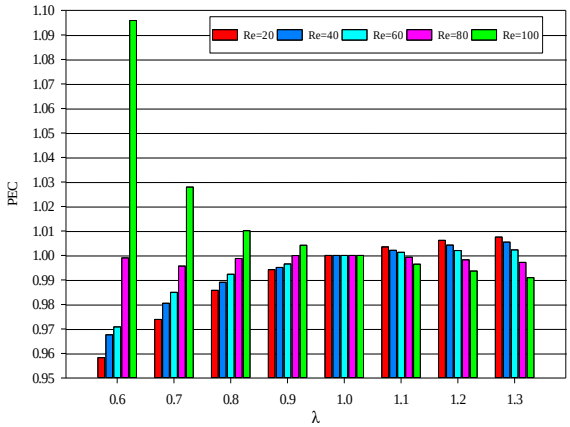

Figure 12. Variations of the PEC versus λ for different Re

7. 4. Effect of H_{ch} and W_{ch} on Heat Transfer and Pressure Drop In this section, variations of the Nu and Δp at various H_{ch} and W_{ch} for Re=20 and 100 were studied. Before presenting the results and analyzing them, it is notable that: according to that the results are presented for a constant Re, according to the definition of Re in Equation (9) and ratio of mass flow rate in Equation (12), with variation of H_{ch} and W_{ch}, mass flow rate changes so that the Re remains constant.

$$\dot{m}_{ch_2}/\dot{m}_{ch_1} = \frac{A_{ch_2} D_{h_1}}{A_{ch_1} D_{h_2}} \quad (12)$$

Figures 13 and 14 show variations of Nu and Δp versus H_{ch} for different values of W_{ch} for Re=20 and Re=100, respectively. The following can be seen from Figures 13 and 14:

By increasing the H_{ch}, the Nu increases at first and decreases slightly at the end. The effect of W_{ch} is more evident in larger values of H_{ch}. As the H_{ch} increases, the effect of W_{ch} on the Nu becomes more evident.

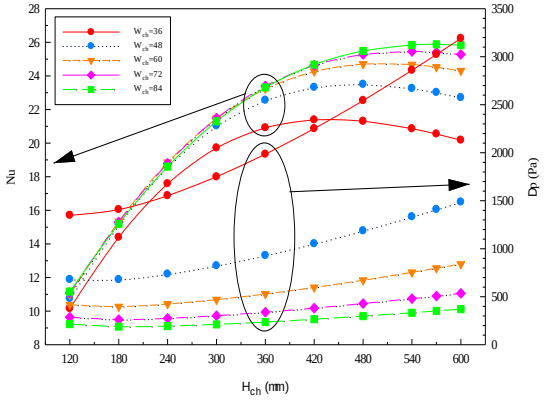

Figure 13. Variations of the Nu and Δp versus H_{ch} for different W_{ch} for Re=20

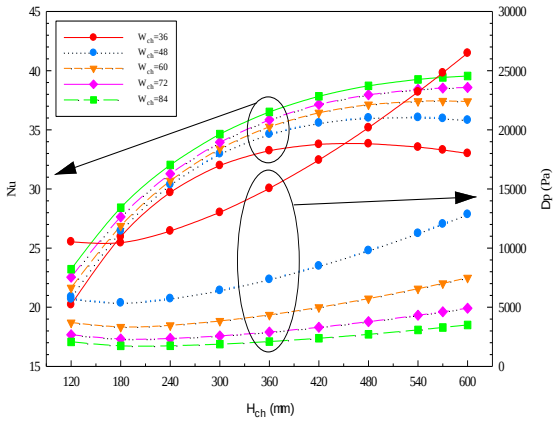

Figure 14. Variations of the Nu and Δp versus H_{ch} for different W_{ch} for Re=100

Also, as the W_{ch} increases, the Nu_{max} is obtained at a greater H_{ch}. Table 1 shows Nu_{max} and coresponding H_{ch}, for which Nu_{max} is obtained for various W_{ch} at Re=20 and Re=100. As can be seen, by increasing Re, the Nu_{max} is received at a higher H_{ch}. According to Figure 13, for W_{ch}=48μm to W_{ch}=84μm, as the H_{ch} increases, Δp first decreases slightly and then increases, so that at higher H_{ch} and lower W_{ch}, a more severe pressure drop is observed.

TABLE 1. Nu_{max} for various W_{ch} at Re=20 and Re=100

W_{ch}(μm)	Re	Nu_{max}	H_{ch}(μm)
36	20	21.38	420
	100	33.83	480
48	20	23.51	480
	100	36.06	540
60	20	24.71	480
	100	37.45	570
72	20	25.46	540
	100	38.59	600
84	20	25.89	570
	100	39.55	600

But for W_{ch}=36μm, an increasing trend is observed from the beginning to the end. The same trend is observed for Figure 14, with the difference that, firstly, for all values of the W_{ch}, the Δp first decreases slightly and then increases, and secondly, the Δp values are higher than Re=20.

7. 5. Effect of Channel Height and Channel width on PEC Figure 15 shows variations of PEC with repect to H_{ch} for various W_{ch} at Re=20 and Re=100. Table 2 shows PEC_{max} and corresponding H_{ch} for various W_{ch} and Re. According to Figure 15, for all Re, by increasing H_{ch}, PEC increases at first and then decreases. By

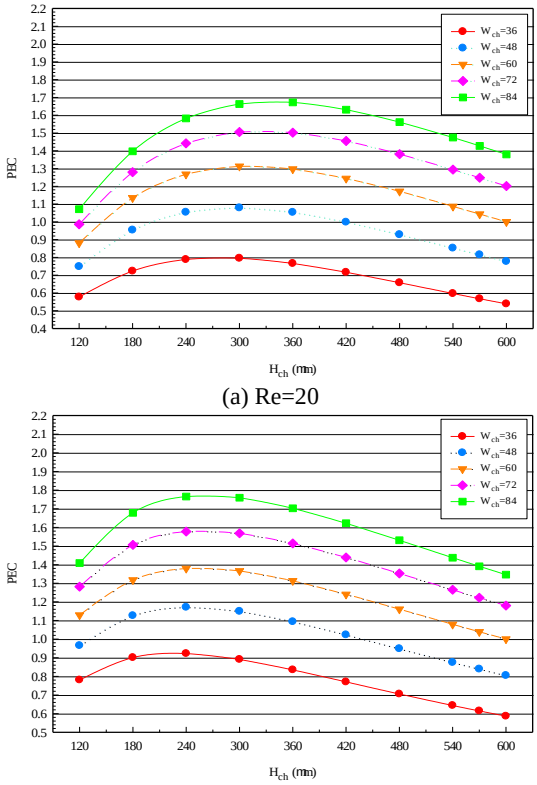

(a) Re=20

(b) Re=100

Figure 15. PEC for different values of H_{ch} and W_{ch} for (a) Re=20 and (b) Re=100

TABLE 2. Maximum PEC and corresponding H_{ch} for various W_{ch} and Re

	PEC				
W_{ch}(μm)	Re=20	Re=40	Re=60	Re=80	Re=100
36	0.795 at H_{ch}=300	0.867 at H_{ch}=240	0.896 at H_{ch}=240	0.915 at H_{ch}=240	0.922 at H_{ch}=240
48	1.078 at H_{ch}=300	1.118 at H_{ch}=300	1.136 at H_{ch}=240	1.160 at H_{ch}=240	1.171 at H_{ch}=240
60	1.313 at H_{ch}=300	1.328 at H_{ch}=300	1.342 at H_{ch}=300	1.358 at H_{ch}=240	1.379 at H_{ch}=240
72	1.505 at H_{ch}=300	1.504 at H_{ch}=300	1.520 at H_{ch}=300	1.541 at H_{ch}=300	1.578 at H_{ch}=240
84	1.672 at H_{ch}=360	1.650 at H_{ch}=300	1.671 at H_{ch}=300	1.705 at H_{ch}=300	1.765 at H_{ch}=240

comparing the PEC for Re=20 and 100, it is observed PEC is increased with W_{ch}; this increase is more for middel H_{ch} (PEC_{max} is occured between H_{ch}=240µm and H_{ch}=300µm).

Similar trend for above parameter were reported by previous reserchers [8-10]. But study on the PEC was arly are considered in the previous investigations. Based on the obatined results, one can say current investigation is more applicable than previous reported investigation.

8. CONCLUSION

The effect of λ, H_{ch}, and W_{ch} at Re=20 to 100 on the heat transfer and flow field characteristics including Nu, Δp, and PEC for laminar flow regime of water in the MMHS have been simulated numerically. The results showed that:

- As the Re increases, the thermal and hydrodynamic boundary layer thickness is reduced, and therefore, the heat transfer rate is increased.
- For H_{ch}=600µm, W_{ch}=60µm, W_f=60µm and λ=0.6, by increasing the Re from 20 to 100, the maximum temperature of the microchannel floor is reduced from 311.3K to 306.3K.
- For H_{ch}=600µm, W_{ch}=60µm, W_f=60µm and Re=100, by decreesing λ from 1 to 0.6, the maximum temperature of the microchannel floor is reduced from 307.8K to 306.3K.
- By increasing in λ, the amount of Nu and Δp is reduced.
- For low Re, it is better to choose a λ>1 and for high Re, choose a λ<1. The highest PEC is for Re=100 and λ=0.6 (PEC =1.095).
- By increasing Re, the Nu_{max} is occured at higher H_{ch} (for example at W_{ch}=84µm, Nu_{max}=25.89 for H_{ch}=570µm & Re=20, and Nu_{max}=39.55 for H_{ch}=600µm & Re=100).
- At the highest H_{ch} and the least W_{ch}, the highest Δp is observed (Δp =2700Pa at H_{ch}=600µm & W_{ch}=36µm).
- By increasing W_{ch}, PEC increases. PEC_{max} is occured at middel H_{ch}; between H_{ch}=240µm and H_{ch}=300µm.

To complete this work and in the future simulations, the authors intend to consider the micro-scale phenomena such as charge accumulation or slip effect near the walls. Also, investigation about the effect of using hybrid nanofluids as a cooling fluid to improve the cooling in this system is of interest to the authors.

9. REFERENCES

1. Bailina, F., Pei, Z., Ganghan, H., YanJun, W., "Research on Properties of Fluid Pressure Drop for Electric Vehicle IGPT Pin Fin Heat Sink", ***International Journal of Engineering, Transactions A: Basics,*** Vol. 28, No. 4, (2015), 627-633. DOI: 10.5829/idosi.ije.2015.28.04a.18.
2. Sarabandi, A. H., Jabari Moghadam, A., "Slip Velocity in Flow and Heat Transfer of Non-newtonian Fluids in Microchannels", ***International Journal of Engineering, Transactions A: Basics,*** Vol. 30, No. 7, (2017), 1054-1065. DOI: 10.5829/ije.2017.30.07a.15.
3. Safikhani, H., Shaabani, H., "Numerical Simulation of Frost Formation in Interrupted Micro Channel Heat Sinks Considering Microfluidic Effects in Slip Regime", ***International Journal of Engineering, Transactions C: Aspetcs,*** Vol. 33, No. 12, (2020), 2556-2562. DOI: 10.5829/ije.2020.33.12c.17
4. Tan, H., Wu L., Wang, M., Yang Z., Du, P., Heat transfer improvement in microchannel heat sink by topology design and optimization for high heat flux chip cooling, ***International Journal of Heat and Mass Transfer***, Vol. 129, (2019). https://doi.org/10.1016/j.ijheatmasstransfer.2018.09.092
5. Adeyemi, T.S., Rufus, D.O., "Analytical Development of an Improved Inflow Performance Relationship (IPR) Model for Solution Gas Drive Reservoirs," ***Journal of Human, Earth and Future***, Vol. 2, No. 2, (2021). Doi: 10.28991/HEF-2021-02-02-04.
6. Kapeller, H., Dvorak, D., Šimić, D., "Improvement and Investigation of the Requirements for Electric Vehicles by the use of HVAC Modeling, ", ***HighTech and Innovation Journal***, Vol. 2, No. 1, (2021). Doi: 10.28991/HIJ-2021-02-01-07
7. Kermani, E., "Manifold micro-channel cooling of photovoltaic cells for high efficiency solar energy conversion", M.S. Thesis, University of Maryland, (2008).
8. Escher, W., Michel, B., Poulikakos, D., "A novel high performance ultra-thin heat sink for electronics, ***International Journal of Heat and Fluid Flow***, Vol. 31, (2010), 586-598. https://doi.org/10.1016/j.ijheatfluidflow.2010.03.001.
9. Cetegen, E., "Force Fed Microchannel High Heat Flux Cooling Utilizing Microgrooved Surface", Dissertation submitted to the Faculty of the Graduate School of the University of Maryland, College Park, in partial fulfillment of the requirements for the degree of Doctor of Philosophy, (2010).
10. Kasten, P., Zimmermann, S., Tiwari, M.K., Michel, B., Poulikakos, D., "Hot water-cooled heat sinks for efficient data center cooling: towards electronic cooling with high exergetic utility", ***Frontiers in Heat and Mass Transfer***, Vol. 1, (2010). http://dx.doi.org/10.5098/hmt.v1.2.3006.
11. Boteler, L., Jankowski, N., McCluskey, P., Morgan, B., "Numerical investigation and sensitivity analysis of manifold microchannel coolers", ***International Journal of Heat and Mass Transfer***, Vol. 55, (2012) 7698-7708. https://doi.org/10.1016/j.ijheatmasstransfer.2012.07.073.
12. Husain, A., Kim, K.Y., "Design Optimization of Manifold Microchannel Heat Sink Through Evolutionary Algorithm Coupled with Surrogate Model", ***IEEE Transactions on Components, Packaging and Manufacturing Technology***, Vol. 3, (2013), 617-624. https://doi.org/ 10.1109/95.588554.
13. Sarangi, S., Bodla, K.K., Garimella, S.V., Murthy, J.Y., "Manifold microchannel heat sink design using optimization under uncertainty", ***International Journal of Heat and Mass Transfer***, Vol. 69, (2014), 92-105. https://doi.org/10.1016/j.ijheatmasstransfer.2013.09.067.
14. Arie, M.A., Shooshtari, A.H., Dessiatoun, S.V., Ohadi, M.M., "Thermal optimization of an air-cooling heat exchanger utilizing manifold-microchannels", Fourteenth Intersociety Conference on Thermal and Thermomechanical Phenomena in Electronic Systems (ITherm), (2014), 807-815. https://doi.org/ 10.1109/ITHERM.2014.6892364

15. Arie, M.A., Shooshtari, A.H., Dessiatoun, S.V., Al-Hajri, E., Ohadi, M.M., "Numerical Modeling and Thermal Optimization of a Single-phase Flow Manifold-Microchannel Plate Heat Exchanger", ***International Journal of Heat and Mass Transfer***, Vol. 81 (2015), 478-489. https://doi.org/10.1016/j.ijheatmasstransfer.2014.10.022.
16. Yue, Y., Mohammadian, S.K., Zhang, Y., "Analysis of performances of a manifold microchannel heat sink with nanofluids", ***International Journal of Thermal Sciences***. Vol. 89, (2015), 305-313. https://doi.org/10.1016/j.ijthermalsci.2014.11.016.
17. Andhare, R.S., Shooshtari, A.H., Dessiatoun, S.V., Ohadi, M.M., "Heat Transfer and Pressure Drop Characteristics of a Flat Plate Manifold Microchannel Heat Exchanger in Counter Flow Configuration", ***Applied Thermal Engineering***. Vol. 96, (2016), 178-189. https://doi.org/10.1016/j.applthermaleng.2015.10.133.
18. Li, S.N., Zhang, H.N., Li, X.B., Li, Q., Li, F.C., Sang, S. Q., Joo, W., "Numerical study on the heat transfer performance of non-Newtonian fluid flow in a manifold microchannel heat sink", ***Applied Thermal Engineering***, Vol. 115, (2017), 1213-1225. https://doi.org/10.1016/j.applthermaleng.2016.10.047.
19. Arie, M.A., Shooshtari, A.H., Rao, V.V., Dessiatoun, S.V., Ohadi, M.M., "Air-Side Heat Transfer Enhancement Utilizing Design Optimization and an Additiv Manufacturing Technique", *ASME*, ***Journal of Heat Transfer***, Vol. 139, (2017). https://doi.org/10.1115/1.4035068.
20. Drummond, K.P., Back, D., Sinanis, M.D., Janes, D.B., Peroulis, D., Weibel, J.A., Garimella, S.V., "A Hierarchical Manifold Microchannel Heat Sink Array for High-Heat-Flux Two-Phase Cooling of Electronics", ***International Journal of Heat and Mass Transfer***, Vol. 117, (2018), 319-330. https://doi.org/10.1016/j.ijheatmasstransfer.2017.10.015.
21. Ju, X., Xu, C., Zhou, Y., Liao, Z., Yang, Y., "Numerical investigation of a novel manifold micro-pin-fin heat sink combining chessboard nozzle-jet concept for ultra-high heat flux removal", ***International Journal of Heat and Mass Transfer***, Vol. 126, (2018), 1206-1218. https://doi.org/10.1016/j.ijheatmasstransfer.2018.06.059.
22. Zhang, H., Li, S., Cheng, J., Zheng, Z., Li, X., Li, F., "Numerical study on the pulsating effect on heat transfer performance of pseudoplastic fluid flow in a manifold microchannel heat sink", ***Applied Thermal Engineering***. Vol. 129, (2018), 1092-1105. https://doi.org/10.1016/j.applthermaleng.2017.10.124.
23. Jung, K.W., Kharangate, C.R., Lee, H., Palko, J., Zhou, F., Asheghi M., Dede, E.M., Goodson, K.E., "Embedded cooling with 3D manifold for vehicle power electronics application: Single-phase thermal-fluid performance", ***International Journal of Heat and Mass Transfer***, Vol. 130 (2019), 1108-1119. https://doi.org/10.1016/j.ijheatmasstransfer.2018.10.108.
24. Tiwari, R., Andhare, R.S., Shooshtari, A., Ohadi, M.M., "Development of an Additive Manufacturing-Enabled Compact Manifold Microchannel Heat Exchanger", ***Applied Thermal Engineering***. Vol. 147, (2019), 781-788. https://doi.org/10.1016/j.applthermaleng.2018.10.122.
25. Luo, Y., Li, J., Zhou, K., Zhang, J., Lia, W. , "A numerical study of subcooled flow boiling in a manifold microchannel heat sink with varying inlet-to-outlet width ratio", ***International Journal of Heat and Mass Transfer***, Vol. 139, (2019), 554-563. https://doi.org/10.1016/j.ijheatmasstransfer.2019.05.030.
26. Yang, M., Cao, B.Y., "Numerical study on flow and heat transfer of a hybrid microchannel cooling scheme using manifold arrangement and secondary channels", ***Applied Thermal Engineering***. Vol. 159, (2019). https://doi.org/10.1016/j.applthermaleng.2019.113896.
27. Drummond, K.P., Weibel, J.A., Garimella, S.V., "Two-phase flow morphology and local wall temperatures in high-aspect-ratio manifold microchannels", ***International Journal of Heat and Mass Transfer***, Vol. 153, (2020). https://doi.org/10.1016/j.ijheatmasstransfer.2020.119551.
28. Luo, Y., Zhang, J., Li, W., "A comparative numerical study on two-phase boiling fluid flow and heat transfer in the microchannel heat sink with different manifold arrangements", ***International Journal of Heat and Mass Transfer***, Vol. 156, (2020). https://doi.org/ 10.1016/j.ijheatmasstransfer.2020.119864.
29. Yang, M., Li, M.T., Hua, Y.C., Wang, W., Cao, B.Y., "Experimental study on single-phase hybrid microchannel cooling using HFE-7100 for liquid-cooled chips", ***International Journal of Heat and Mass Transfer***, Vol. 160, (2020). https://doi.org/10.1016/j.ijheatmasstransfer.2020.120230.
30. Luo, Y., Li, W., Zhang, J., Minkowycz, W.J., "Analysis of thermal performance and pressure loss of subcooled flow boiling in manifold microchannel heat sink", ***International Journal of Heat and Mass Transfer***, Vol. 162, (2020). https://doi.org/10.1016/j.ijheatmasstransfer.2020.120362.
31. Bergman, T.L., Avine, A.S., Incropera, F.P., Dewitt, D.P., Fundamentals of Heat and Mass Transfer, Seventh ed., John Wiley & Sons, Hoboken, 2011.
32. Glassbrenner, C.J., Slack, G.A., "Thermal Conductivity of Silicon and Germanium from 3K to the Melting Point", ***Physical Review***. Vol. 134, (1964), 1058-1069. https://doi.org/10.1103/PhysRev.134.A1058.
33. Ghorbani, M., Salimpour, M.R., Vafai, K., "Microchannel thermal performance optimization utilizing porous layer configurations", ***International Journal of Heat and Mass Transfer***, Vol. 133, (2019), 62-72. https://doi.org/10.1016/j.ijheatmasstransfer.2018.12.063.

Persian Abstract

چکیده

در این تحقیق، انتقال حرارت و رفتار جریان سیال در حالت آرام و برای سیال آب در یک چاه حرارتی میکروکانال منیفولدی بطور عددی شبیه‌سازی شده است. برای اطمینان از صحت روش عددی، نتایج با اطلاعات تجربی موجود مقایسه شده است. در شبیه‌سازی جریان سیال و انتقال حرارت، خواص ترموفیزیکی سیال آب و سیلیکون متغیر (وابسته به دما) در نظر گرفته شده است. تاثیر نسبت طول ورودی به خروجی جریان، ارتفاع میکروکانال و پهنای میکروکانال به عنوان پارامترهای مستقل در اعداد رینولدز ۲۰ تا ۱۰۰ بر جریان سیال و انتقال حرارت بررسی شده است. نتایج نشان داد که در چاه حرارتی میکروکانال منیفولدی، جت برخوردی بر سطح پایین کانال، رشد لایه مرزی هیدرودینامیکی و حرارتی را محدود می‌کند و در نتیجه نرخ انتقال حرارت افزایش می‌یابد. همچنین با افزایش عدد رینولدز و ثابت نگه داشتن ابعاد هندسی، نرخ انتقال حرارت افزایش می‌یابد. بر اساس نتایج حاضر، برای اعداد رینولدز کوچک، بهتر است $\lambda > 1$ و برای اعداد رینولدز بزرگ $\lambda < 1$ انتخاب شود. در محدوده مطالعه، برای اعداد رینولدز کوچک، ماکزیمم معیار ارزیابی عملکرد (PEC_{max}) در $H_{ch}=300\mu m$ بدست می‌آید و برای اعداد رینولدز بزرگ در $H_{ch}=240\mu m$ بدست می‌آید. برای اعداد رینولدز ۲۰ تا ۱۰۰، ماکزیمم معیار ارزیابی عملکرد برابر با ۱.۷۶۵ و در $Re=100$ و $H_{ch}=240\mu m$ بدست می‌آید.